Aggregate size effects on the mechanical behaviour and on the gas permeability at damaged state of cement-based materials with and without slag

Aurélie Fabien, Marta Choinska, Stéphanie Bonnet, Arnaud Pertue, Abdelhafid Khelidj

Aggregate size effects on the mechanical behaviour and on the gas permeability at damaged state of cement-based materials with and without slag

Aurélie Fabien[a,b], Marta Choinska[a],Stéphanie Bonnet[a], Arnaud Pertue[a] and Abdelhafid Khelidj[a]

[a]Université de Nantes, GeM UMR CNRS 6183 - Institut de Recherche en Génie Civil et Mécanique, IUT Saint-Nazaire, Saint-Nazaire cedex, France

[b]COMUE Normandie Université, Laboratoire ESITC, ESITC Caen, Epron, France

The purpose of this article is to investigate the effects of aggregate size on the mechanical and mass transfer behavior of concrete. The experimental work is carried out using three types of materials: microconcrete, concrete and macroconcrete. All these materials chosen have the same water-to-cement ratio and the same aggregate volume fraction. They are prepared using two different cement types, CEM I and CEM III as alternative binder for environmental considerations. In order to study the evolution of the microstructure due to changes in aggregate size, gas permeability, water and mercury porosity measurements are first carried out on sound materi-als. Then, some specimens of the formulated materials are subjected to a series of controlled uniaxial compression cycles in the pre-peak phase to achieve intended damage levels corresponding to 30, 60 or 80% of their compressive strength, respectively. Gas permeability is then measured on the damaged specimens after unloading. For all the materials, the results suggest that mechanical strength decreases and gas permeability increases when aggregate size increases. Use of cement CEM III with slag show an increase of mechanical properties and reducing the strain. But the slags seems to be more sensitive to the drying that can be increase the strain and strength characteristics. Moreover, the results also show that the effect of compressive damage on permeability may be separated from the effect of aggregate size using two distinct functions. As a result, such behaviour, independent of cement type, is a major advantage for concrete modelling.

1. Introduction

In quasi-brittle materials like concrete fracture occurs within a finite cracking initiation area. Macrocracking is the result of progressive damage of the material, in which microcracks first appear diffusely, then coalesce and form the crack. The size of the resulting cracking initiation area is not dependent on the structural size but is controlled by a local heterogeneity parameter (aggregate size).Concrete behavior, therefore, yields size effects (Bazant, 2004a; Pijaudier-Cabot et al., 2004). The characterization of these effects can be used to correlate laboratory test results with the structural behaviour, which is essential for durability assessment, for instance.

Two different approaches can be considered for the investigation of size effects. The first one is based on changes in specimen size for the same material. According to Bazant (1991, 2004b; Bazant & Pang, 2007), strain localization induces size effect on cracking energy. More recently, some research works (Alam, 2011; Alam et al., 2015) on damage mechanisms on beams of various sizes, using digital image correlation and acoustic emission methods, underline the size effects on strains in the post peak phase. Other studies are also carried out to highlight size effects on compressive strength (Dehestani et al., 2014). Barr and El-Baden (1999), using samples of various sizes, also demonstrate the effect of size on both drying shrinkage and weight loss.

The second approach is based on changes in aggregates size for the same specimen size. Some studies showed that there would be no significant difference in terms of the compressive strength due to the size of aggregate (Jiang et al., 2017). But the most of studies confirm the aggregate size effects on different parameters, such as compressive strength (Del Viso et al., 2008; Khaloo et al., 2010; Majeed, 2011; Malaikah, 2005; Sim et al., 2013; Tokyay & Ozdemir, 1997; Yazici & Sezer, 2007), tensile strength, elastic modulus and cracking energy (Elices & Rocco, 2008; Petersson, 1980; Tasdemir et al., 1996; Wolinski et al., 1987).

Contrary to the works of Szczesniak et al. (2013) on compressive strength and of Elices and Rocco (2008) on tensile behaviour, Meddah et al. (2010), when varying the size of the aggregates, observe an increase in the compressive strength of concrete when the maximal size of coarse aggregates increases. Vu et al. (2011) studies on the effects of aggregate size and cement paste volume under extreme stress in triaxial compression also confirm the size effects on the elastic modulus and the Poisson's ratio.

Compressive strength and compressive fracture energy are among the most important mechanical characteristics of the concrete structure (Nakamura et al., 2018). Aggregate size affects cracking energy: the greater the aggregate size, the greater the cracking energy (Bazant & Oh, 1984; Chen & Liu, 2004; Walker & Bloem, 1961). These findings contrast with those obtained by Duan et al. (2006, 2007). Current results differ because many parameters must be taken into account.

However, all these studies highlight the effects of size on the mechanical properties of concrete, and to a lesser extent on the transport properties. Basheer et al. (2005) observe the effect of aggregate size on concrete permeability, which is directly influenced by the number, type and size of the pores in concrete. Concrete porosity depends on aggregate size, when the size of coarse aggregate and the proportion of larger size coarse aggregate increases in a mix, there is an associated increase in air permeability. The study conducted by Ozbay (2010) shows the influence of aggregate size on chloride ion ingress into concrete. This research also demonstrates that there is an optimal aggregate size (average 16 mm) to minimize chloride ion permeability.

Because concrete transport properties changes with damage state (Choinska et al., 2007; Djerbi et al., 2008; Djerbi Tegguer et al., 2013; Picandet et al., 2001), the possibility that both damage and aggregate size are coupled with the evolution of transport properties cannot be excluded. However, little or no research is focusing on this subject in the literature. Consequently, the present article addresses this issue. Moreover in the context of environmental considerations as the production of Portland cement which generates large amount of CO_2 emissions, promoting alternative binders, in which clinker is replaced by mineral admixtures, offers a promising solution. Blast Furnace Slag, considered as byproducts, is used in this study as alternative binder as it may contribute to improve the long-term performance of concrete with higher resistance to aggressive agents (Ben Fraj et al., 2012; Fraj et al., 2019; Papadakis, 2000).

In order to examine the problem, six different concrete formulations are presented for two different types of cement, CEM I and CEM III. The aggregate volume fraction is kept constant while the aggregate size changes from 12 to 20 mm. The experimental setup and procedures are described and the main results discussed: stress, strain (longitudinal and transverse), Poisson's ratio and damage evolutions due to compressive loading for different mean aggregate size in case of materials with or without slag. Changes in gas permeability, measured before and after loading/unloading cycles, as a function of aggregate size and the cement type, are also examined.

2. Experimental program

2.1. Materials

Six cement-based materials are formulated using two different types of cement, CEM I and CEM III, to investigate the differences between both. The compositions of the both cements are given in Table 1.

Table 1. Chemical composition of both cements.

	% (by weight)	
Compounds	CEM I 52.5N CE PM ES CP2 NF	CEM III/A 52.5 L CE PM ES CP1 NF
CaO	64.76	50.50
SiO2	21.18	29.20
Fe2O3	4.28	1.00
Al2O3	3.56	8.20
SO3	2.55	2.74
MgO	0.81	5.00
K2O	0.25	0.29
Na2O	0.16	0.28
Specific surface (cm^2/g)	3680	4186
Density ( )	3.2	2.97
Main compounds (Bogue's equation) % by weight		
Clinker	98.5	36
Slag		62
C3S	66	69.1
C2S	8.6	7.1
C3A	2.9	11.8
C4AF	12.4	6.2
Filler	1.5	2
Gypsum	3.1	2.4
Anhydrite		2.4

The casted materials are in the XS2 environmental exposure category (NF EN 206-1). In order to study aggregate size effect on concrete properties, these materials have the same water-to-cement ratio ($W/C = 0.48$) and the same aggregate volume fraction (Table 2).

Limestone aggregates are used. All the aggregates come from one quarry, and each type of aggregate comes from one delivery. All the particles in different sizes have, therefore, similar shapes.

The volume of aggregate remains 659 L/m^3 (65.9% of the total volume),while the amount of aggregates of various sizes varies for each concrete material. Three types of cement-based materials are then realized: microconcrete (only sand and medium aggregate), concrete (sand, medium aggregate and coarse aggregate) and macroconcrete (sand and coarse aggregate).The obtained materials are presented in Figure 1.

In order to examine aggregate size effects on concrete behaviour, a new parameter is defined: the mean aggregate size (Table 3). This parameter is obtained by using the weighted average method on the aggregate size distributions shown in Figure 2.

The mean aggregate size (MAS) was calculated with the formula described below.

$$\mathbf{MAS} = \left[\sum \left(\frac{[\emptyset_{i+1} + \emptyset_i]}{2}\right) * (\%\boldsymbol{P}_{i+1} \quad \%\boldsymbol{P}_i)\right] /100 \tag{1}$$

With: $\emptyset_{i+1}$: upper sieve diameter for an interval i

$\emptyset_i$: lower sieve diameter for an interval i

For i varing between .0063 mm and 28 mm.

$\%P_{i+1}$: cumulative percentage of aggregate passing from the $i+1$ sieve

$\%P_i$: cumulative percentage of aggregate passing from the i sieve

The aggregate specific surface is calculated, assuming the aggregates as perfectly spherical and using the mass percentage of each aggregate type given in Table 3. For coarse aggregates, the mass percentage is the ratio of the mass of coarse aggregate to the total mass of aggregate. A decrease in the mean aggregate size causes an increase in the aggregate specific surface.

2.2. Experimental program of the research work

Figure 3 describes the experimental procedure applied. Fourteen 110 × 220-mm cylindrical specimens are prepared from a single batch for each mix, casted in PVC moulds and compacted using a mechanical

Table 2. Concrete constituents and mix proportions.

Constituents (kg/m^3)	Microconcrete	Concrete	Macroconcrete
Cement CEM I 52.5 PM ES or CEM III/A 52.5 PM ES	350	350	350
Sand 0 4 mm	867.8	867.8	867.8
Medium aggregate 4 12 mm	1009	432	
Coarse aggregate 12 20 mm		561.2	981.4
Aggregate volume fraction		65.9 %	
Water		168	
Superplasticizer (solid content 20%)		1.71	

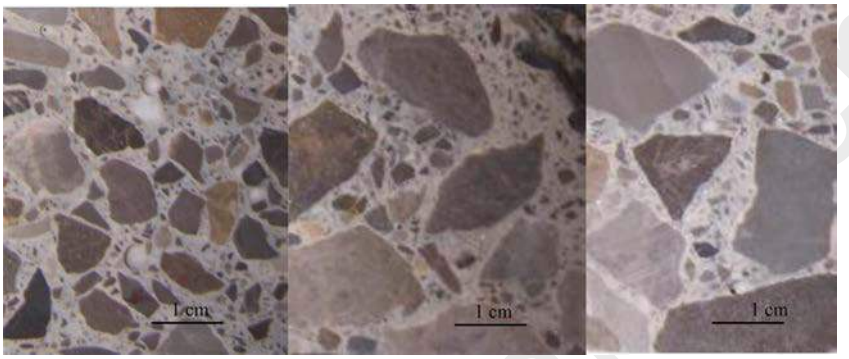

Figure 1. Sawn sections of CEM III microconcrete (left), concrete (middle) and macroconcrete (right).

Table 3. Characteristics of the aggregate skeleton.

Constituents	Microconcrete	Concrete	Macroconcrete
Mean Aggregate Size (MAS) (mm)	5.3	7.8	9.7
Aggregate Specific surface (cm^2/g)	9170	9017	8902
Mass percentage (%) Sand 0 4 mm	46.2	46.6	46.9
Mass percentage (%) Medium aggregate 4 12 mm	53.8	23.2	
Mass percentage (%) Coarse aggregate 12 20 mm		30.2	53.1

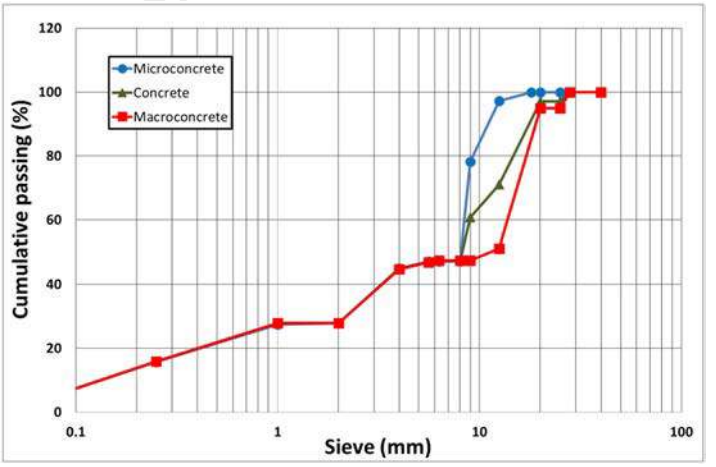

Figure 2. Aggregates size curves for the three concrete formulations.

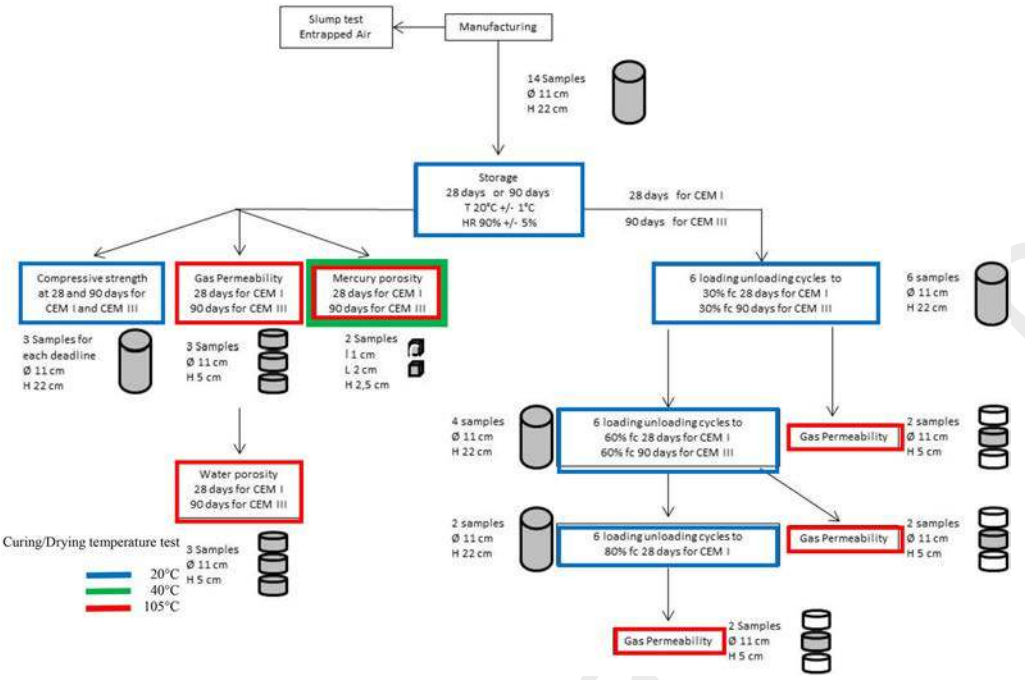

Figure 3. Experimental program of the research work.

vibrator. The specimens are moist cured at $20 \pm 1\,^{\circ}C$ and $90 \pm 5\%$ relative humidity for 28 days and 90 days.

Eight cylindrical specimens are used to determine the characteristics of the sound materials: compressive strengths at 28 days and 90 days, gas permeability, water porosity and mercury porosity at 90 days. Compressive strength tests are carried out on six cylindrical specimens, three at 28 days and three at 90 days for each material.

In order to measure the gas permeability of the undamaged concrete products, for each mix, one concrete cylindrical specimen is cut using a diamond blade saw to obtain three 50-mm thick disc specimens. These specimens are dried at 80 °C during two weeks and at 105 °C to a constant mass (during approximately two weeks). The same three 50-mm thick discs are used to measure the open porosity by water saturation under vacuum conditions.

The pore analysis using the Mercury Intrusion Techniques is carried out using another 110×220-mm cylindrical specimen. Two $1 \times 2 \times 2.5\text{-cm}^3$ samples are cut from the cylindrical specimen and oven-dried at 40 °C until constant mass. Mercury porosity measurements are carried out on these two small cubes using AUTOPORE IV (Micromeritics).

The six remaining cylindrical specimens are partially damaged under the action of compressive loads applied at three levels of loading. Gas permeability is then measured after unloading. Two cylindrical specimens, with the same loading level applied, are cut to obtain two 50-mmthick discs, one from each cylindrical specimen. These discs are dried at 80 °C for two weeks and at 105 °C to a constant mass. The mean value is displayed in the figures found in Subsection 3.5.

2.3. Mechanical damage procedure

Prior to loading, the specimens are polished to produce a plane and cleaned surface. They are equipped with a strain cell using one circumferential and three axial extensometers placed by intervals of 120° (Figure 4).

All the specimens are damaged under cyclic uniaxial compressive loading. This method is used to generate uniform damage and is already acknowledged in the literature (Saito & Ishimori, 1995). The tests

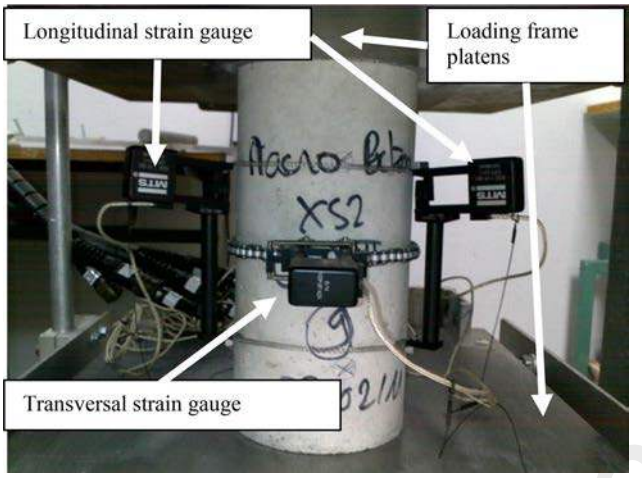

Figure 4. The mechanical device equipped with the strain cell.

are conducted with a load control system using a hydraulic loading frame with a maximum capacity of 1500 kN. The loading-unloading rate is kept constant and equal to 2 kN/s.

Different load levels are applied to the specimens, corresponding to 30% (referred to as 'Loading level 0'), 60% (referred to as 'Loading level 1') and 80% (referred to as 'Loading level 2') of the reference compressive strength, respectively. The reference strength corresponds to the maximal stress:

- at 28 days for materials with CEM I
- at 90 days for materials with CEM III.

However, because most concrete used for current structures is designed for loading below 66% fc (NF EN 1992-1-1, Eurocode 2), the study is restricted to the 'Loading level 1'. Only the CEM I materials, which are the reference ones, are tested up to the 'loading level 2'.

At loading levels0 and 1, six loading-unloading cycles are applied to the specimens. At loading level 2, only three cycles are applied in order to minimize a risk of any potential specimen failure, and therefore, deterioration of the extensometers.

To validate the experimental procedure proposed here, two specimens of the same CEM I concrete are submitted to loading levels 0, 1 and 2. Figure 5 displays relative stress versus longitudinal and transverse strains. Figure 6 shows the apparent Poisson's ratio (transverse strain divided by the longitudinal strain) trend during the loading-unloading cycles. These two Figures confirm the good repeatability of the damage tests. For convenience in the analysis, in Section 3 'results and discussion', the values displayed in the Figures are the mean values of both specimens obtained during the last loading-unloading cycle for each loading level.

One of the parameters used in this study is the experimental damage evaluation based on elastic modulus losses. The elastic modulus E_0 of sound concrete corresponds to the slope on the stress-longitudinal strain response curve of the specimens during the unloading phase between 30% and 0% of the maximal loading value. The elastic modulus of damaged concrete E_d are calculated with the unloading curve after both loading levels 1 and 2. Since E_0 and E_d denote the elastic modulus of sound and damaged concrete, respectively, the damage 'd' can be defined from the elastic modulus relative loss (Mazars, 1984) as:

$$d = \frac{E_0 \quad E_d}{E_0} \tag{2}$$

where E_0 is the initial elastic modulus calculated after Loading level 0, and E_d is the elastic modulus after the other loading levels.

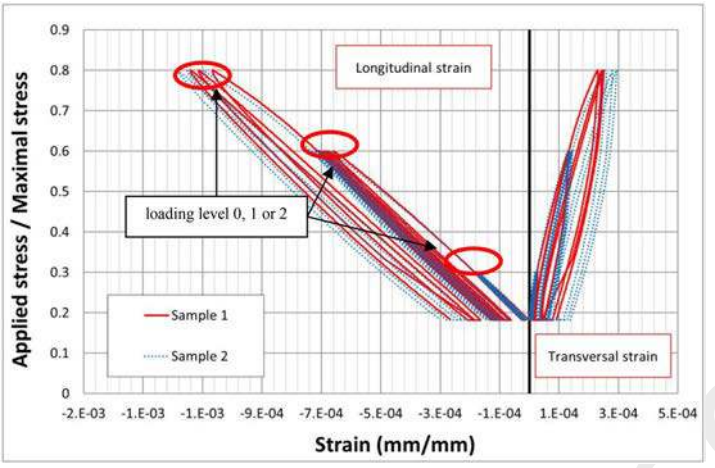

Figure 5. Relative stress vs. strains for two CEM I concrete specimens.

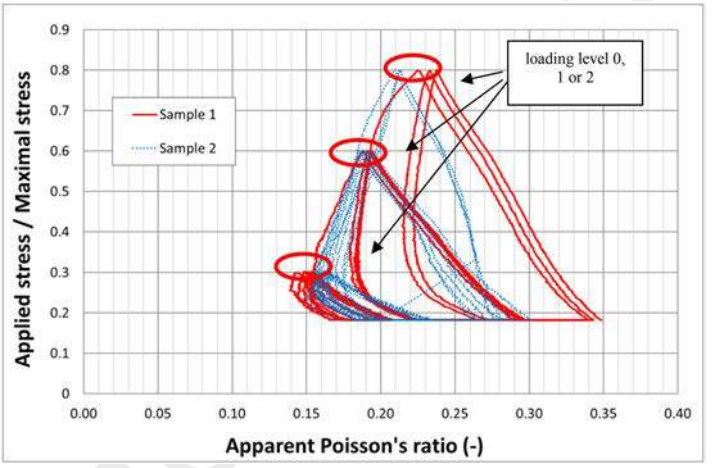

Figure 6. Relative stress vs. the apparent Poisson's ratio for two CEM I concrete specimens.

2.4. Permeability measurements

Because water content affects measurement, drying the sample discs prior to any gas permeability measurements is necessary (Bazant et al., 1987; Kameche et al., 2014; Kollek, 1989; Picandet et al., 2001).The drying procedure is that described in Subsection 2.2. The discs are then cooled during 48 h in a desiccator at 20 °C before measurement can be started.

The device used to test gas permeability is detailed in Figure 7. It includes a permeability cell based on the Cembureau cell (Kollek, 1989; XP P 18-463, 2011). The tests are performed using an inert gas (dry nitrogen, N_2). To ensure the uniaxial flow of gas and to prevent parasitic gas leakage, the lateral face of the cylindrical specimens is covered with aluminum wrap. The specimen tested, held in place by a fitted collar is then confined during the tests (0.5 MPa). This confining pressure is quite low, equal for all the specimens (sound and cracked ones) and, for this reason, has a slight impact of the measurements (Choinska & Niknezhad, 2020). The gas is injected at the lower surface of the specimen at pressure P_i, between 0.3 and 0.1 MPa (relative values) while its upper side remains at atmospheric pressure (P_{atm}). To estimate the intrinsic permeability (Klinkenberg, 1941; Picandet et al., 2001), all the tests include some flow measurements at five differential pressures (0.10, 0.15, 0.20, 0.25 and 0.30 MPa, respectively). The injection pressure is maintained until the gas flow stabilizes. The pressure and the flow rates are recorded during the test. Flow rates are measured upstream and downstream of the measurement system using

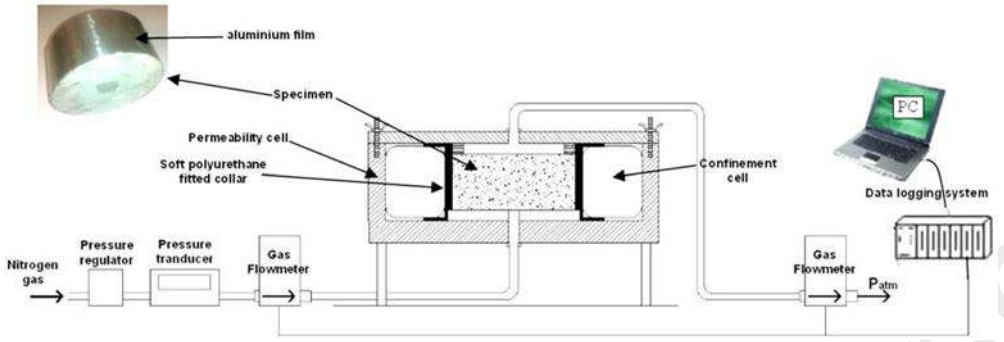

Figure 7. Schematic layout of the permeability device.

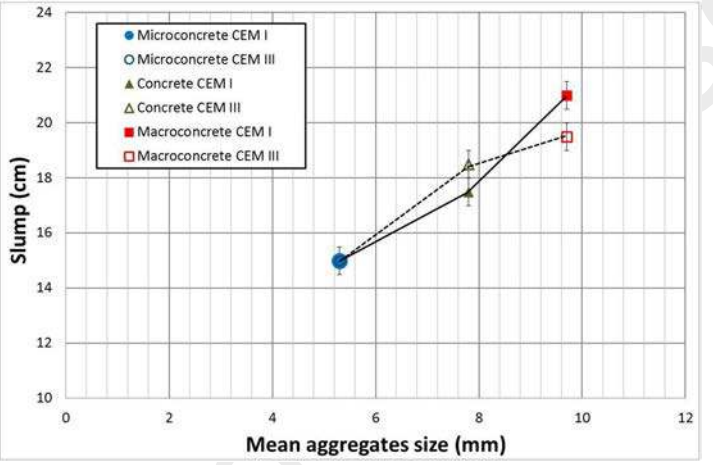

Figure 8. Slump values according to mean aggregate size.

thermal mass flowmeters with different capacities used to convert the mass flow rate into an equivalent volumetric gas flow rate in normalized conditions (P_0, T_0).

Using Darcy's law and mass balance equation, the apparent permeability k_a (m^2) can be determined. Using the thermal mass flowmeters, the resulting solution takes the form:

$$k_a(T_a) = \frac{2Q_i(T_0, P_0)P_0 \frac{T_a}{T_0} \mu(T_a)L}{S({P_i}^2 \quad {P_{\text{atm}}}^2)} \tag{3}$$

where P_i: injection pressure, T_a: room temperature, $P_0 = 1013.105\,P_a$, $T_0 = 273\,K$, Q_i (T_0, P_0): equivalent volumetric gas flow rate in normalized conditions (m^3/s), μ: nitrogen dynamic viscosity (Pa.s), L: specimen height (m), S: specimen surface (m^2).

The intrinsic permeability can be determined using Klinkenberg's regression of the apparent permeability (Klinkenberg, 1941).

3. Results and discussion

3.1. Influence of aggregate size on concrete slump

Figure 8 displays concrete slump values according to mean aggregate size for the six tested materials. CEM I and CEM III materials show the same tendency and no effect of cement type is noted. An increase in slump of approximately 15% is observed between microconcrete and concrete and between concrete and macroconcrete. This tendency coincides with the increase in mean aggregate size and the decrease in the specific surface area of these aggregates. Aggregate size significantly affects workability (Pereira et al., 2009; Piotrowska, 2013). The increase observed here may be due to the amount of cement paste

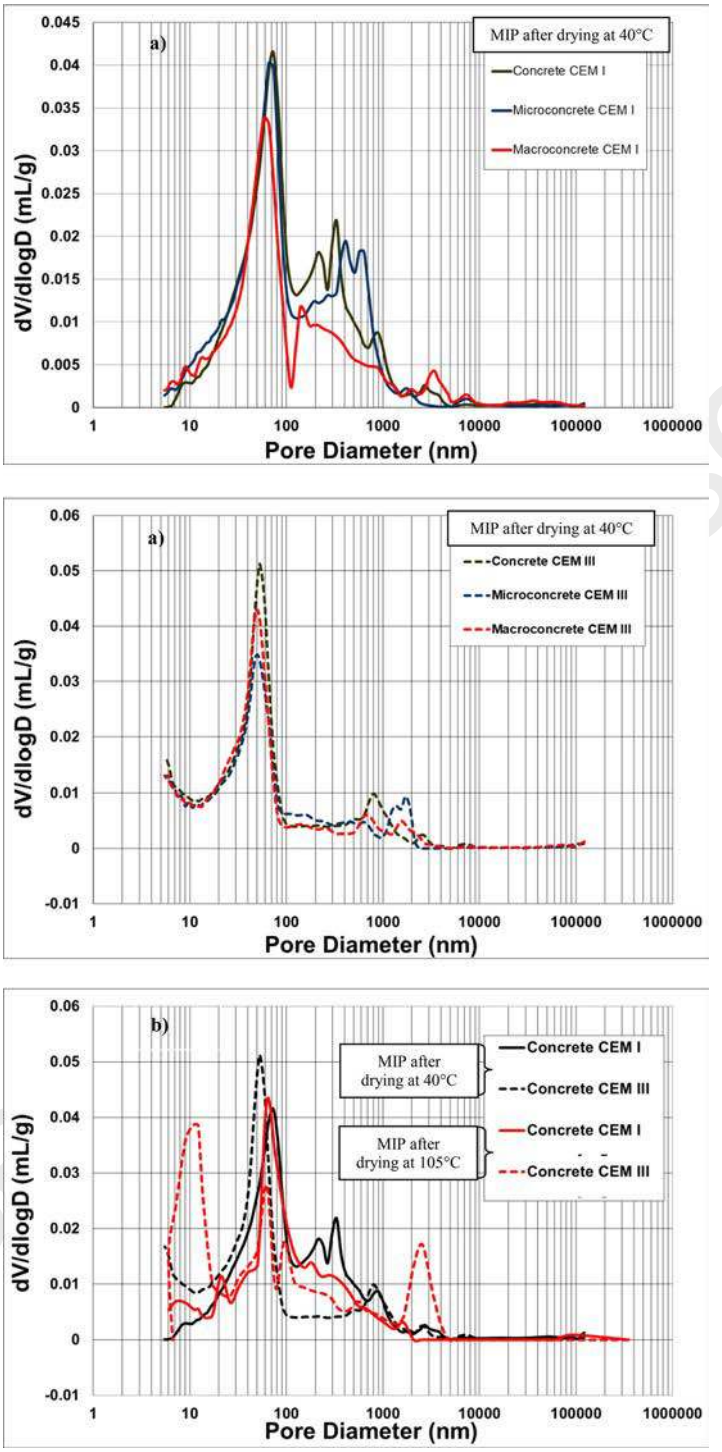

Figure 9. Differential pore size distribution using mercury intrusion porosity. (a) For CEM I materials (up) and CEM III materials (down) after drying at 40 °C, (b) drying effects on CEM I and CEM III materials ('with drying' means drying at 105 °C).

filling intergranular spaces. In the case of small aggregate size, the paste must cover a larger specific surface area, which decreases the amount of paste between the aggregates. Another explanation for the observed trend maybe aggregate water consumption. Walker and Bloem (1961) show that aggregate size

affects water consumption: the larger the aggregates, the lower the demand for water. A smaller specific surface area absorbs less water and, consequently, slump values are higher. The specific surface area also influences the interfacial transition zone (ITZ) of the aggregate-cement paste (Gao et al., 2005) Aggregate size and volume fraction may influence bonding forces localized in the ITZ (Al-Khazraji, 2017).

3.2. Influence of aggregate size and cement type on concrete porosity

The mercury intrusion porosity (MIP) measurements are carried out on two $1 \times 2 \times 2.5\,cm^3$ small cubes, within which care was taken to avoid main aggregates. Both cubes are dried at 40 °C until constant mass prior to any measurements. The MIP data confirm the good repeatability of the results between both cubes. The mean data are given in Figure 9.

Variations of the pore size distribution with different aggregate size can be obtained from the pore size distribution curves (Figure 9(a)). Some differences are observed among the three different types materials and the two types of cement. As shown in Figure 9(a) with an increasing aggregate size, the peak values of the pore size distribution increased. More finest pores are found in concrete and microconcrete than macroconcrete mainly in the case of CEM I. The volume percentages of the pore diameter ($200 < d < 900$ nm for CEM I and $900 < d < 1200$ nm for CEM III) increase significantly in the case of micrococrete and concrete regarding macroconcrete.The largest pore size ranges between 200 and 900 nm for CEM I and between 900 and 1200 nm for CEM III but with a lowest volume percentage for CEM III. The threshold pore diameter depends on the type of cement: 70 nm for CEM I and 50 nm for CEM III. As already shown by Ben Fraj et al. (2012) who compares total water porosity and water vapour absorption isotherms for the two binders after drying at 60 °C, the mortar obtained with cement CEM III is finer than the CEM I mortar when drying is not aggressive for slag binder.

To complement this analysis, a comparison of the drying effect on mercury porosity results for both types of cement is made (Figure 9(b)). Only two CEM I and CEM III concrete specimens are tested after two different drying temperatures (40 °C, as before, and 105 °C, as for the permeability study). Indeed, high temperature drying at 105 °C affects the microstructure of the CEM III concrete due to larger thermal incompatibility between the cement paste with slag CEM III and limestone aggregate, in comparison to the cement paste CEM I and the same aggregate (Sato & Mizobuchi, 2018). This incompatibility results in formation of new voids and microcracks ($1000\,nm < d < 8000\,nm$) around the aggregates as also indicated by Asamoto et al. (2018), which demonstrate in increase of porosity as well as in change of pores distribution (see Figures 9(b) and 10).

Figure 10(a) shows the total porosity values obtained by water saturation under vacuum conditions after drying the 50-mm thick discs at 105 °C (see Figure 3). The values displayed are the averages of three discs. The porosities observed for both types of materials show no similar trends: for instance, for CEM I materials, water porosity is highest in macroconcrete whereas it is the lowest for CEM III one. However, these differences are generally small. Nevertheless, the CEM I materials present lower water porosity values than CEM III.

Concerning the total porosity values obtained by MIP after drying at 40 °C (Figure 10(b)), the differences between CEM I and CEM III materials for each type of concrete products are more representative and in accordance with the results obtained about the pore size distribution. Indeed, the opposite trend is observed: the CEM III materials present lower mercury porosity values than CEM I ones. This is still due to drying effects: the most temperature-sensitive materials are the CEM III ones, as already highlighted by Figure 9(b). After drying at low temperature, the concretes with cement CEM III have lower total porosities than those of the CEM I concretes because of the finer mortar (Figure 9(b)). The reactivity of the slag enhances the hydration of the clincker which leads to low a decrease in size of pores. The microstructure is then denser and richer in fine pores.

3.3. Influence of aggregate size on compressive strength

Compressive strength at 28 and 90 days for all the materials tested is summarized in Table 4. The values displayed are the averages of three experimental results.

For the two types of cement studied here, compressive strength increases when mean aggregates size decreases.

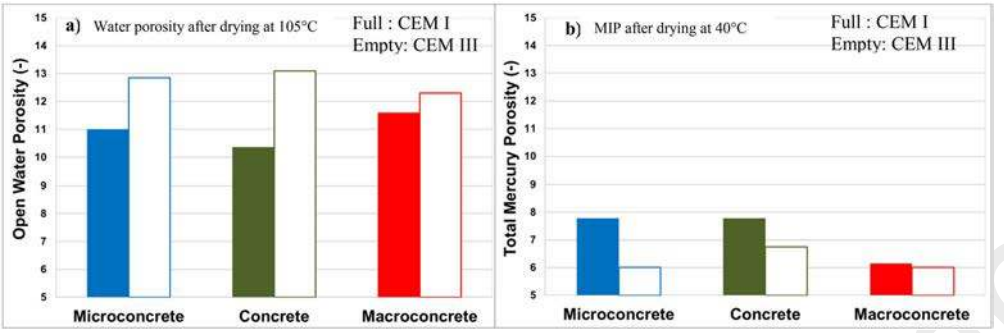

Figure 10. Total materials porosity. (a) Open water porosity after drying at 105 °C, (b) mercury porosity after drying at 40 °C.

Table 4. Compressive strength for the six tested materials.

Materials	Microconcrete		Concrete		Macroconcrete	
Cement	CEM I	CEM III	CEM I	CEM III	CEM I	CEM III
Strength at 28 days (MPa)	59.8	59	55.5	57	50.6	54.5
Strength at 90 days (MPa)	63.4	67	62.2	64.3	53.5	58.3

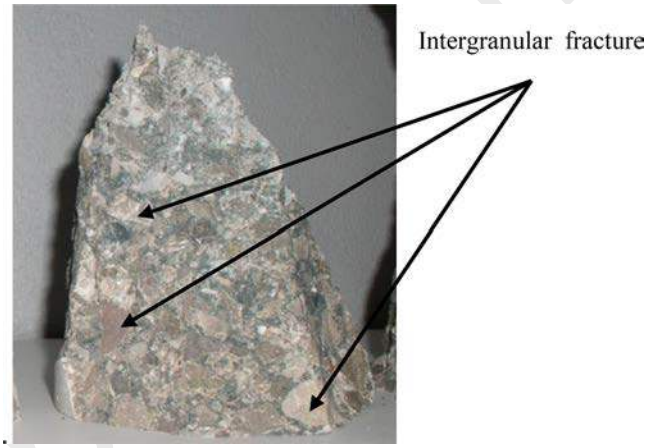

Figure 11. Failure mode of CEM Iconcrete.

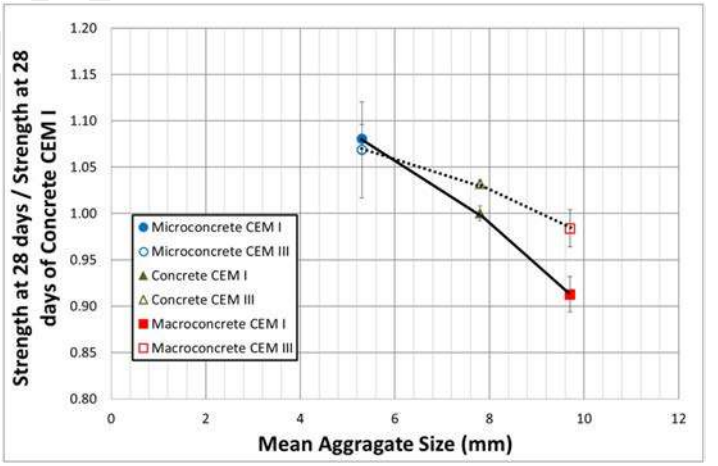

Figure 12. Strength vs. mean aggregate size at 28 days.

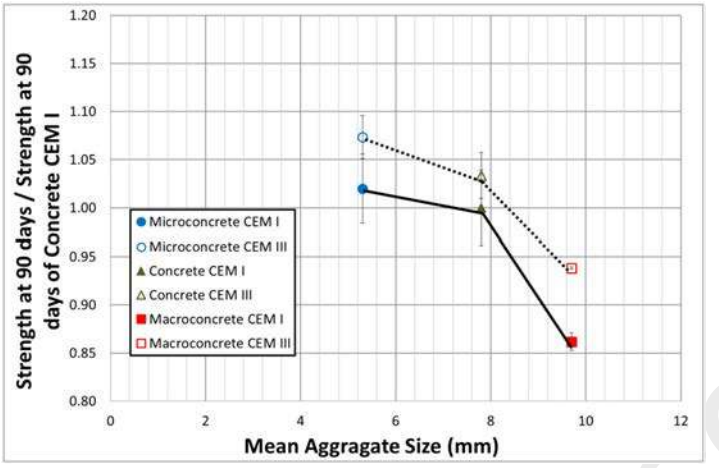

Figure 13. Strength vs. mean aggregate size at 90 days.

During compression testing, concrete fracture is observed with three distinct zones: in the paste, in the aggregates and in the intergranular zone. The most common type for the tested materials is the intergranular fracture (Figure 11), common for limestone aggregates and especially present here for the concretes and the microconcretes. A strong cohesion, despite mechanical incompatibilities between paste and aggregates, exists within these materials, with the largest aggregate specific surface. In any case, the aggregate specific surface area should influence the interfacial transition zone (ITZ) of aggregate-cement paste (Gao et al., 2005). Usually, as the mechanical properties of aggregates and paste are quite different, the risk of damage is more important at the interface between aggregates and paste (Mehta, 1986; Shah & Sankar, 1987). However, with this type of aggregates, calcareous, the ITZ is small and appears not impacted.

For convenience in the comparison of the materials and the plotting of compressive strength as a function of mean aggregate size, relative strength values are used. The relative values are the ratio of the values obtained for each material to the strength value obtained for the reference CEM I concrete.

For both types of cement, relative compressive strength decreases as mean aggregate size increases, for the both tested materials ages: 28 and 90 days (Figures 12 and 13, respectively). These evolutions, however, are not linear. Concretes and microconcretes values, for instance, present a steady trend, with relatively close values at 90 days. Macroconcretes values exhibit the most significant decrease in strength, compared to others materials. This sharper fall can be explained by the nonoptimal arrangement of aggregates due to the absence of particles between 4 and 12 mm, which leads to the presence and then damage of largest intergranular spaces.

Float-Goble and Cohen (1999) carried out mechanical compressive strength tests on cement-based material shaving similar formulations as the materials tested here. These authors demonstrate that the larger the aggregate specific surface area, the higher mechanical strength. The present results show in general a parallel trend and highlight the relevance of aggregate size on the mechanical behaviour of materials.

When comparing CEM I and CEM III materials, compressive strength is almost higher for the CEM III materials. The reason for these higher values is due to the improvement in the CEM III material compactness. CEM III cement, indeed, has a larger specific surface, and therefore, smaller particles than the CEM I cement (Table 1). These particles fill the material porosity, which result in a more compact material, when not subjected to drying at 105 °C as explained in Subsection 3.2.

3.4. Influence of aggregate size on mechanical behaviour

Figures 14 and 15 show the evolution of the residual and maximal longitudinal and transverse strain obtained for the last cycle of each loading level. CEM I macroconcrete has the largest residual and maximal strains, and exhibits greater damage. The same observation can be made for longitudinal or transverse strain, either residual or maximal. As previously underlined, macroconcrete is the material, for

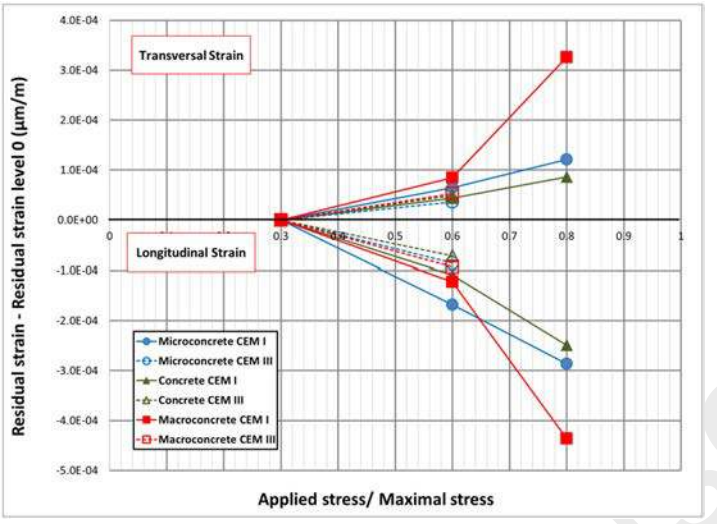

Figure 14. Residual strains.

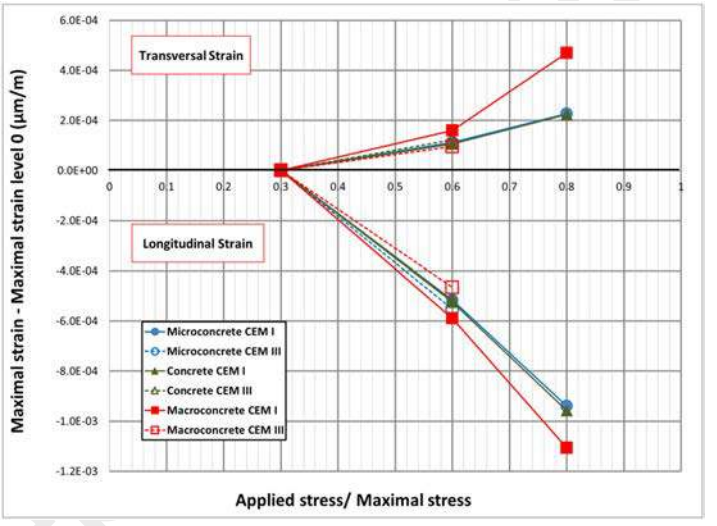

Figure 15. Maximal strains.

which the generation of crack requires the lowest energy compared to the other two materials. This explains why it exhibits more residual nonreversibles.

For all the tested materials, strains increase progressively with loading level. At loading level 0 (applied stress/Maximal stress = 30%), the variations between the materials are very small. For both types of cement, concrete and microconcrete behaviours are very close. As regards CEM I materials at all the loading levels, the largest strains are observed in macroconcrete and the weakest in microconcrete. On the contrary, the opposite trend applies for CEM III materials but with lowest loading as only level 0 and 1 loadings were applied to CEM III specimens.

Microconcrete behaviour can be explained through its granular composition (Tables 2 and 3). Because microconcrete is composed of mainly small aggregates, the specific surface of the microconcrete aggregates at constant volume is larger than those of concrete and macroconcrete. The specific surface probably affects not only compressive strength values obtained but also strain values. CEM I microconcrete is mechanically stronger and exhibits less strain than CEM I macroconcrete. This macroconcrete, because of the nonoptimal arrangement of its aggregates, requires a larger volume of paste to bond aggregates. In

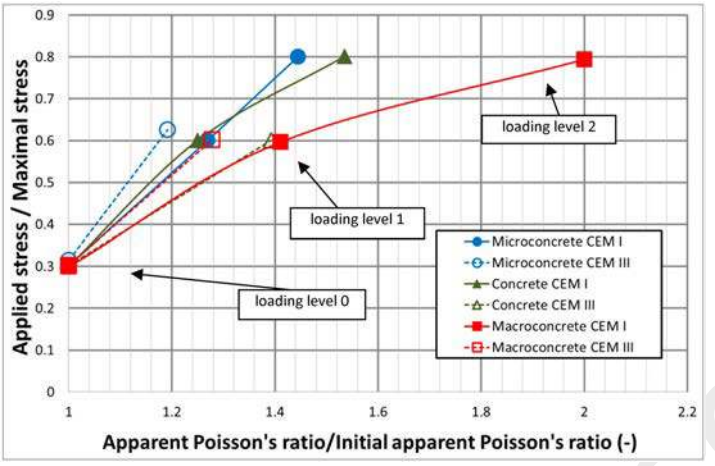

Figure 16. Stress vs. Poisson's ratio.

CEM III materials, the substitution of clinker by slag produces a more compact paste resulting in a decrease in the total porosity and a refinement of the porous network (Figures 9(a) and 10(b)). As regards strain results, this densification of paste has a greater effect than the reduction of the specific surface area and the nonoptimal granular arrangement. CEM III strain measurements are lower for macroconcrete than microconcrete as well as strength results.

Figure 16 presents the relative stress in relation to the relative apparent Poisson's ratio during the last cycle for all the loading levels and six materials tested. The initial apparent Poisson's ratio is determined for loading level 0 (Figure 6). The values increase with the loading level. Poisson's ratios are plotted according to the mean aggregate size so that all the different materials tested can be compared (Figure 17). The macroconcrete presents the sharper rise compared with the other two materials. This result may be accounted for by the capacity of macroconcrete to generate strong transverse strain variations resulting in significant cracking parallel to the loading direction. This material exhibits ductile fracture in contrast to concrete and microconcrete, which appear to be more fragile. Macroconcrete cracking energy is lower than that of the other two materials. These observations are in good agreement with the results found in the literature (Elices & Rocco, 2008; Petersson, 1980; Tasdemir et al., 1996). In these studies, the cracking energy is measured on concrete specimens made of aggregates of different sizes according to the RILEM TC-50 standard. Petersson (1980) addresses changes in cracking energy of CEM I concretes using indirect tensile testing. The same approach is used by Elices and Rocco (2008) for CEM III concretes. They obtain results similar to those found by Tasdemir et al. (1996). However, the latter, contrary to the two others carries out compression tests on sample cubes of CEM I concretes.

In order to compare the tested materials, their compressive damage has been investigated. Damage is plotted as a function of the loading level in Figure 18. At the initial loading level 0, CEM III and CEM I materials behave similarly and no damage is recorded for both materials. The level of damage increases with loading almost linearly for all the materials. However, damage of CEM III materials is systematically lower than for the CEM I materials. Furthermore, whatever the type of cement used, concrete and microconcrete evolutions are very similar. Nevertheless, damage of macroconcrete is greater than this of concrete and microconcrete, especially for the CEM III materials.

Damage evolution as a function of mean aggregate size is plotted in Figure 19. At loading level 0, CEM III and CEM I values are superimposed. Like in Figure 18, concrete and microconcrete behaviours are similar for both types of cement. The similarity of the results is probably due to their granular arrangement, which is optimized in comparison with macroconcrete. Macroconcrete exhibits the greatest damage (cf. Figures 18 and 19). Indeed, the thickness of the paste between aggregates is greater in macroconcrete than in concrete or microconcrete. This difference in structure may explain the results obtained because cracks occur mainly in the paste (Rougelot et al., 2010). Since macroconcrete has a larger paste width between its aggregates, it has a larger area allowing the appearance of cracks unlike other formulations.

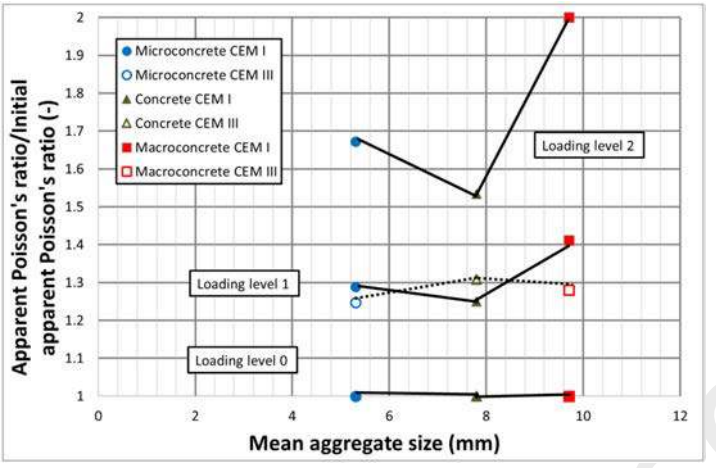

Figure 17. Poisson's ratio vs. Mean aggregate size.

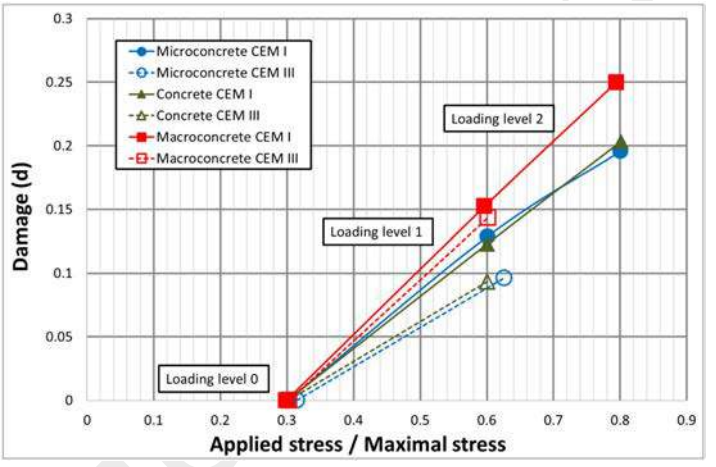

Figure 18. Damage vs. loading level.

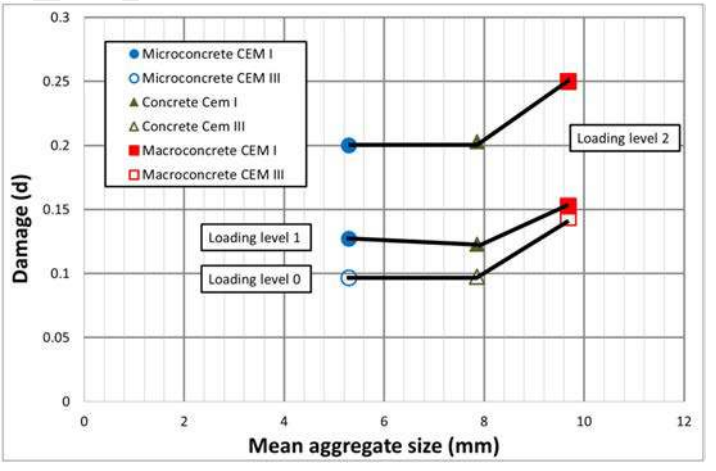

Figure 19. Damage vs. mean aggregate size.

Table 5. Initial intrinsic permeability values.

Materials	Microconcrete		Concrete		Macroconcrete	
Cement	CEM I	CEM III	CEM I	CEM III	CEM I	CEM III
Initial permeability (m^2)	3.1 E 17	4.2 E 17	3.6 E 17	8.3 E 17	1.0 E 16	1.5 E 16

3.5. Influence of aggregate size on transport properties: interaction with damage

This section presents gas permeability results for sound and damaged materials. The intrinsic permeability values obtained using Klinkenberg regression (Klinkenberg, 1941) on the apparent permeabilities, measured using four different inlet pressures, are presented. The permeability values, summarized in Table 5, are averages for undamaged materials of three specimens.

Care and Derkx (2011) have established a correlation between aggregate size and gas permeability: the bigger the aggregate diameter, the greater the gas permeability. The same trend has been obtained by Wu et al. (2015) who confirm the increase in permeability with the aggregate diameter. In undamaged conditions, microconcrete permeability is the lowest and macroconcrete the highest. Such behaviour can probably be explained by the formation of a connected network of microcracks due to the shrinkage around the coarse aggregates (Rougelot et al., 2010) and consequently to the increase in the initial permeability with aggregate size. The same trend can be observed for the apparent permeabilites. Grassl et al. (2010) also confirm that an increase in aggregate size increases permeability values, but not other results were found in the literature.

Figure 20 display the initial permeability as a function of mean aggregate size. These results are partially in accordance with the strength values (Table 4 and Figures 12 and 13). Macroconcrete materials with the lowest strength present the highest gas permeability values. However, the gas permeability of the CEM III materials is higher than the CEM I materials, which is contrary to the trend observed for strength values. This may be explained by the sensitivity of CEM III materials to high drying temperatures as explained in Subsection 3.2, before the permeability test. Indeed, the specimens are dried at 105 °C before testing using the Cembureau permeameter. Nevertheless, these results are in good accordance with the water porosity results obtained with the same specimens after completion of the gas permeability measurements (Figure 10(a)).

According to the analysis proposed by Picandet et al. (Ozbay, 2010), in the pre-peak phase, measuring the permeability as a function of damage instead of strain or stress, is more consistent. So, in order to analyze the effect of the applied load on permeability, permeability versus damage is plotted in Figure 21. There is in fact no common trend, probably due to the combined effects of mechanical damage and aggregate size. In order to examine this problem, damage and aggregate size effects are studied separately.

Using Figures 21 and 22 is plotted and represents the relative permeability, corresponding to the ratio of the intrinsic permeability of the damaged material, $kv(d)$, to the intrinsic permeability of the same sound material, $kv0$, versus the damage, d. Damage corresponds to the values shown in Figures 18 and 19. An exponential and nonmaterial dependent evolution is observed with a kinetics more important for macroconcrete which has an intrinsic permeability of uncracked concrete larger than the microconcrete and concrete (exponential curve fitting to the experimental data). The exponential relationship 'f: $kv(d)/kv(0) = 0.95 \exp(1.1^{*}d)$' is given in Figure 22. It means that mechanical damage is still relevant of microstructural changes occurring in the pre-peak phase, for any aggregate size tested at any loading level tested. This observation is in agreement with the experimental results obtained by other researchers (Choinska et al., 2007; Djerbi Tegguer et al., 2013; Picandet et al., 2001). However, the comparison of the values of permeability and of damage with results obtained by other researchers yields some slight differences probably due to the flow geometry and the mechanical loading applied. In this study, an uniaxial flow was used as opposed to radial flow which was applied by Choinska et al. (2007). The method of determining the damage that we have chosen is the loss of static modulus of elasticity of the central part of the specimen. In Picandet et al. (2001) and Djerbi Tegguer et al. (2013), concrete cylinders were tested under uniaxial compression between 60% and 90% of the ultimate strength and each load level was being sustained for varying periods up to 2 h (Djerbi Tegguer et al., 2013). Gas permeability seems to be more sensitive to damage in the case of sustained loading applied to concrete specimen as $kv(d)/kv0$ increases by a factor of 10 in Djerbi's paper while $kv(d)/kv0$ increases by a factor of 1.5 in the case of

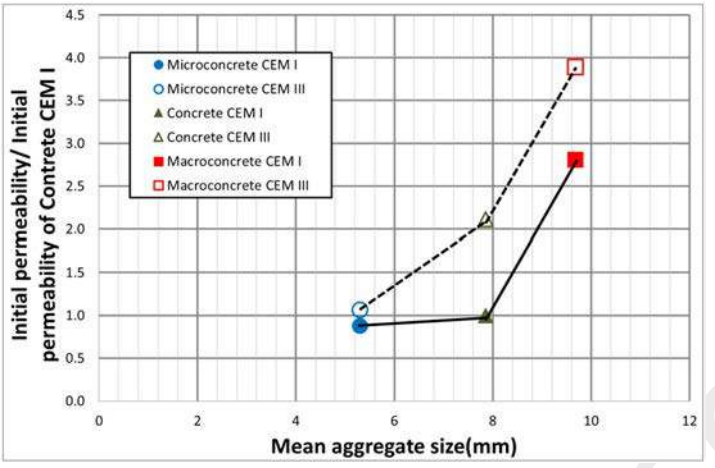

Figure 20. Initial intrinsic permeability vs. mean aggregate size.

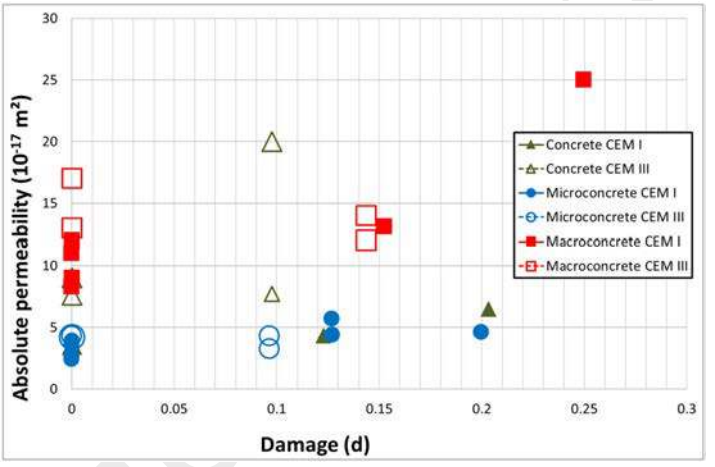

Figure 21. Intrinsic permeability vs. damage.

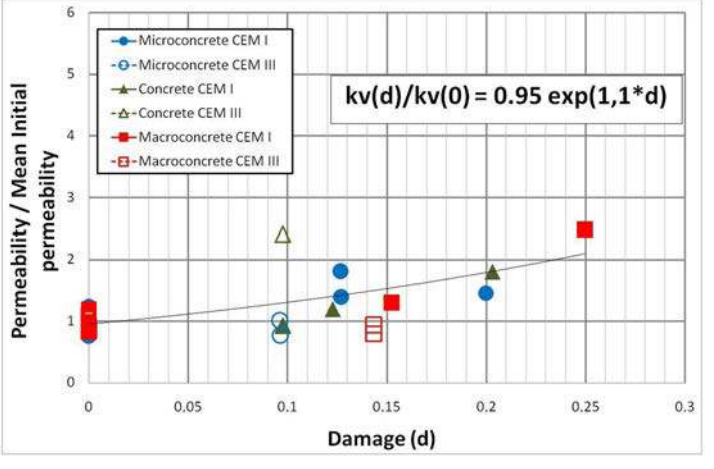

Figure 22. Relative intrinsic permeability vs. mechanical damage.

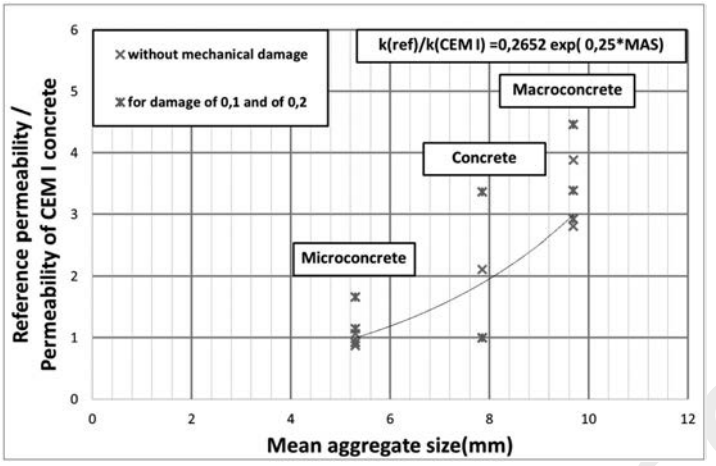

Figure 23. Relative intrinsic permeability vs. aggregate size for different mechanical states.

loading cycles applied to here concrete specimen up to 80% (Figure 22) for about the same measured damage as Djerbi (*d* around 0,15). The crack propagation seems to be quite different between the two typed of loading; a sustained loading seems to induce more connected patterns in which the gas can propagate.

Once the effect of damage on relative permeability is identified, the effect of aggregate size on permeability for all the levels of damage is examined here (Figure 23). As shown in Figure 20, the permeability of a sound material increases with aggregate size. Figure 23 follows the same trend but also includes the data for the damaged materials (exponential curve fitting to the experimental data). Relative permeability is plotted at the initial undamaged state (without mechanical loading) and for damages of 0.1 and 0.2. This relative permeability is the ratio of the permeability of an undamaged or damaged material to the permeability of the equally undamaged or damaged CEM I concrete. We obtain the damaged permeability values from Figure 21 after linear interpolation between the measurements to provide some dates for damages of 0.1 and 0.2. Finally, a common original trend is obtained, depending only on aggregate size and independent from mechanical damage. The exponential relationship '*g*: *k*(ref)/*k*(CEM I) = 0.2652 exp (0.25*MAS)' is given in Figure 23 (with MAS = Mean Aggregate Size).

Therefore, it is possible to conclude that the effect of mechanical damage on cement-based materials permeability can be separated from the effect of aggregate size. Both effects can be represented by two distinct functions f (Figure 22) and g (Figure 23) and the overall permeability evolution can, therefore, be represented by a combination of both functions, presented in Figures 22 and 23.

This original issue, highlighting possible variables separation, represents a strong advantage for concrete modelling, a concept already assumed by Gawin et al. (1999) between damage and temperature effects, and validated experimentally by research works of Choinska et al. (2007), but never proposed before for the aggregate size effects.

4. Concluding remarks

The experimental results discussed in this article highlight the aggregate size significant influence on the mechanical behaviour and gas permeability of cementitious materials in both sound and damage conditions, and whatever the type of cement used, CEM I or CEM III. The concluding remarks can be summarized as follows:

- Microconcrete made of the smallest aggregates, exhibits the highest compressive strength and the lowest gas permeability. Microconcrete strain and damage trends are almost identical to concrete. Damage values are also similar to concrete ones and systematically lower than macroconcrete ones. This is probably due to the fact that microconcrete and concrete have a larger aggregate specific

surface area than macroconcrete, which implies that the contact zone between aggregates and paste is larger. The resulting stronger cohesion then enhances performances.

- On the contrary, macroconcrete has the lowest compressive strength and exhibits the highest damage and permeability values. These results are probably due to its small specific surface (i) and to its increased paste volume between the coarse aggregates (ii). Because cracks (caused by shrinkage or compressive loading) propagate into the paste for limestone aggregate-based materials (De Larrard, 1999), macroconcrete is the most susceptible to cracking.
- The loading level has an important impact on the longitudinal and the transversal strain development. These effects are better visible for the CEM I materials, loaded up to the loading level 2 (80% of compressive strength), than for the CEM III materials, loaded up to the loading level 1 (60% of compressive strength). However, the tendencies remain similar, regardless of cement type: the apparent Poisson's ratio increases with the loading level, getting up to its twice value at the loading level 2 for the macroconcrete CEM I. The loading level is clearly related to the damage, determined as the elastic modulus loss. Here again, the macroconcrete CEM I, but as well the macroconcrete CEM III, are characterized by the highest damage values, 25% and 14%, respectively to the submitted loading level. Damage values for microconcrete and concrete CEM I are similar and are closely followed by the slightly lower but still similar values for the microconcrete and concrete CEM III.
- The CEM III materials (composed of slags) tested in this study are more sensitive to drying temperatures (up to 105 °C) than CEM I materials. However, nondried CEM III materials have higher compressive strength and lower damage than CEM I materials. Nevertheless, once dried at 105 °C, CEM III material gas permeability values are higher than CEM I materials ones at all the states of damage.
- Permeability of all the tested materials varies directly with mechanical damage and with aggregate size. However, it would appear that damage and aggregate size combined effects can be separated using two distinct functions and thus each specific effect highlighted separately. The original approach proposed here, based on the possible separation of problem variables, offers great advantages for concrete modelling and was never used for aggregate size effects estimation. Yet, further studies, with a wider range of aggregate nature and volume fractions, are needed to expand this relationship.

Disclosure statement

No potential conflict of interest was reported by the authors.

Funding

Financial support received from the national network MAREVA (MAquette de REalité Virtuelle d'Aménagement portuaire) and the French Interdepartmental Funds is gratefully acknowledged.

References

Alam, S. Y. (2011). *Experimental study and numérical analysis of crack opening in concrete* [Thèse de doctorat]. École Centrale de Nantes.

Alam, S. Y., Loukili, A., Grondin, F., & Rozière, E. (2015). Use of the digital image correlation and acoustic emission technique to study the effect of structural size on cracking of reinforced concrete. *Engineering Fracture Mechanics*, *143*, 17–31.

Al-Khazraji, H. (2017). *Influence of crack opening, aggregates size and volume fraction on hydro-mechanical properties of concrete in Brazilian splitting test: 3D meso-macro scale modelling and experimental work* [PhD thesis].

Asamoto, S., Yuguchi, R., Kurashige, I., & Chun, P. J. (2018). *Effect of high temperature at early age on interfacial transition zone and material properties of concrete*. RILEM Proceedings PRO 121, SynerCrete'18 International Conference on Interdisciplinary Approaches for Cement-Based Materials and Structural Concrete, Funchal, Portugal.

Barr, B., & El-Baden, A. S. (1999). Shrinkage and weight loss studies in normal and high strength concrete, mechanics of quasi-brittle materials and structures. *Hermes*, 121–137.

Basheer, L., Basheer, P. A. M., & Long, A. E. (2005). Influence of coarse aggregate on the permeation, durability and the microstructure characteristics of ordinary Portland cement concrete. *Construction and Building Materials*, *19*, 682–690.

Bazant, Z. (1991). Size dependance of concrete fracture energy determined by RILEM work-of-fracture method. *International Journal of Fracture*, *51*, 121–138.

Bazant, Z. (2004a). Probability of energetic-statistical size effect in quasi-brittle fracture. *Probabilistics Engineering Mechanics*, *19*, 307–319.

Bazant, Z. (2004b). *Introduction aux effets d'échelle sur la résistance des structures*. Lavoisier.

Bazant, Z., & Pang, S. (2007). Activation energy based extreme value statistics and size effect in brittle and quasibrittle fracture. *Journal of the Mechanics and Physics of Solids*, *55*, 91–131.

Bazant, Z. P., & Oh, B. H. (1984). Déformation of progressively cracking reinforced concrete beams. *American Concrete Institute Journal*, *81*(3), 268–278.

Bazant, Z. P., Sener, S., & Kim, J. K. (1987). Effect of cracking on drying permeability and diffusivity of concrete. *ACI Materials Journal*, *84-M35*, 351–357.

Ben Fraj, A., Bonnet, S., & Khelidj, A. (2012). New approach for coupled chloride/moisture transport in non-saturated concrete with and without slag. *Construction and Building Materials*, *35*, 761–771.

Care, S., & Derkx, F. (2011). Determination of relevant parameters influencing gas permeability of mortars. *Construction and Bulding Materials*, *25*, 1248–1256.

Chen, B., & Liu, J. (2004). Effect of aggregate on the fracture behaviour of high strength concrete. *Construction and Building Materials*, *18*(8), 232–244.

Choinska, M., Khelidj, A., & Chatzigeorgiou, G. (2007). G. Pijaudier-Cabot, Effects and interaction of temperature and stress-level related damage on permeability of concrete. *Concrete and Cement Research*, *37*, 79–88.

Choinska, M., & Niknezhad, D. (2020). *Etude préliminaire – Etude paramétrique relative à la perméabilité au gaz*. PERFDUB French National Project Report No 1A9 (in french). https://www.perfdub.fr/en/

De Larrard, F. (1999). *Structure granulaire et formulation des bétons*. LCPC.

Dehestani, M., Nikbin, I. M., & Asadollahi, S. (2014). Effects of specimen shape and size on the compressive strength of self-consolidating concrete (SCC). *Construction and Building Materials*, *66*, 685–691.

Del Viso, J. R., Carmona, J. R., & Ruiz, G. (2008). Shape and size effects on the compressive strength of high-strength concrete. *Cement and Concrete Research*, *38*, 386–395.

Djerbi, A., Bonnet, S., Khelidj, A., & Baroghel-Bouny, V. (2008). Influence of traversing crack on chloride diffusion into concrete. *Cement and Concrete Research*, *38*, 877–883.

Djerbi Tegguer, A., Bonnet, S., Khelidj, A., & Baroghel-Bouny, V. (2013). Effect of uniaxial compressive loading on gas permeability and chloride diffusion coefficient of concrete and their relationship. *Cement and Concrete Research*, *52*, 131–139.

Duan, K., Hu, X., & Wittmann, F. H. (2006). Scaling of quasi-brittle fracture: Boundary and size effect. *Mechanics and Matérials*, *38*, 128–141.

Duan, K., Hu, X., & Wittmann, F. H. (2007). Size effect on specific fracture energy of concrete. *Engineering Fracture Mechanics*, *74*, 87–96.

Elices, M., & Rocco, C. G. (2008). Effect of aggregate size on the fracture and mechanical properties of a simple concrete. *Engineering Fracture Mechanics*, *75*, 3839–3851.

Float-Goble, C., & Cohen, M. D. (1999). Influence of aggregate surface area on mechanical properties of mortar. *ACI Materials Journal*, *96*(6), 657–662.

Fraj, A. B., Bonnet, S., Leklou, N., & Khelidj, A. (2019). Investigating the early-age diffusion of chloride ions in hardening slag-blended mortars on the light of their hydration progress. *Construction and Building Materials*, *225*, 485–495.

Gao, J. M., Qian, C. X., Liu, H. F., Wang, B., & Li, L. (2005). ITZ microstructure of concrete containing GGBS. *Cement and Concrete Research*, *35*, 1299–1304.

Gawin, D., Majorana, C. E., & Schlefler, B. A. (1999). Numerical analysis of hygro-thermal behaviour and damage of concrete at high temperature. *Mechanics of Cohesive-Frictional Materials*, *4*(1), 37–74.

Grassl, P., Wong, H. S., & Buenfeld, N. R. (2010). Influence of aggregate size and volume fraction on shrinkage induced micro-cracking of concrete and mortar. *Cement and Concrete Research*, *40*, 85–93.

Jiang, C., Wu, W.-F., & Jiang, J.-F. (2017). Effect of aggregate size on stress-strain behavior of concrete confined by fiber composites. *Composite Structures*, *168*(15), 851–862.
Kameche, Z. A., Ghomari, F., Choinska, M., & Khelidj, A. (2014). Assessment of liquid water and gas permeabilities of partially saturated ordinary concrete. *Construction and Building Materials*, *65*, 551–565.
Khaloo, A. R., Mohamadi Shooreh, M. R., & Askari, S. (2010). Size influence of specimens and maximum aggregate on dam concrete: Compressive strength. *ASCE, 21*(8).
Klinkenberg, L. J. (1941). The permeability of porous media to liquids and gases. *API Drilling and Production Practice*, 200–213.
Kollek, J. J. (1989). The determination of the permeability of concrete to oxygen by the Cembureau method - a recommendation. *Materials and Structures*, *22*, 225. https://doi.org/10.1007/BF02472192
Majeed, S. A. (2011). Effect of specimen size on compressive, modulus of rupture and splitting of cement mortar. *Journal of Applied Sciences*, *11*(3), 584–588.
Malaikah, A. S. (2005). Effect of speciment size and shape on the compressive strength of high strength concrete. *Sci, & Technol, 13*(1), 87–96.
Mazars, J. (1984). *Application de la mécanique de l'endommagement au comportement non linéaire et à la rupture du béton de structure* [These de doctorat]. LMT-Universite Paris VI.
Meddah, M. S., Zitouni, S., & Belaabes, S. (2010). Effect of content and particle size distribution of coarse aggregate on the compressive strength of concrete. *Construction and Building Materials*, *24*, 505–512.
Mehta, P. K. (1986). *Concrete. Structure, properties and materials*. Prentice-Hall.
Nakamura, H., Nanri, T., Miura, T., & Roy, S. (2018). Experimental investigation of compressive strength and compressive fracture energy of longitudinally cracked concrete. *Cement and Concrete Composites*, *93*, 1–18.
Ozbay, E. (2010). Influence of aggregate size on the mechanical and transport properties of concretes and concrete-equivalent mortars. *Canadian Journal of Civil Engineering NRC Research Press*, *37*, 1303–1314.
Papadakis, V. G. (2000). Effect of supplementary cementing materials on concrete resistance against carbonation and chloride ingress. *Cement and Concrete Research*, *30*, 291–299.
Pereira, C. G., Castro-Gomes, J., & Pereira de Olivera, L. (2009). Influence of natural coarse aggregate size, mineralogy and water content on the permeability of structural concrete. *Construction and Building Materials*, *23*, 602–608.
Petersson, P. E. (1980). Fracture energy of concrete: Practical performance and experimental result. *Cement and Concrete Research*, *10*(1), 91–101.
Picandet, V., Khelidj, A., & Bastian, G. (2001). Effect of axial compressive damage on gas permeability of ordinary and high-performance concrete. *Cement and Concrete Research*, *31*, 1525–1532.
Pijaudier-Cabot, G., Haidar, K., Omar, M., & Loukili, A. (2004). Non local damage models with evolving internal length: Motivations and applications to coupled problems. *FraMCos 5 - 5th International Conference on Fracture Mechanics of Concrete and Concrete Structures*, *1*, 531–538.
Piotrowska, E. (2013). *Role of coarse aggregates in the triaxial behaviour of concrete: Experimental and numerical analysis* [PhD thesis].
Rougelot, T., Peng, C., Burlion, N., & Bernard, D. (2010). *Cementitious composites during leaching and drying: X-ray microtomography analysis of cracking pattern dependence on size of rigid inclusions, FRAMCOS-7, Fracture Mechanics of Concrete and Concrete Structures*.
Saito, M., & Ishimori, H. (1995). Chloride permeability of concrete under static and repeated compressive loading. *Cement and Concrete Research*, *25*(4), 803–808.
Sato, R., & Mizobuchi, T. (2018). *Guidelines for Cracking of Mass Concrete - Japan Concrete Institute*. RILEM Proceedings PRO 121, SynerCrete'18 International Conference on Interdisciplinary Approaches for Cement-based Materials and Structural Concrete.
Shah, S. P., & Sankar, R. (1987). *Internal cracking and strain softening response of concrete under uniaxial compression*. Center for Concrete and Geomaterials, Northwestern University.
Sim, J., Yang, K., & Jeon, J. (2013). Influence of aggregate size on the compressive size effect according to different concrete types. *Construction and Building Materials*, *44*, 716–725.
Szczesniak, M., Rougelot, T., Burlion, N., & Shao, J.-F. (2013). Compressive strength of cement-based composites: Roles of diameter and watr saturation degree. *Cement and Concrete Composite*, *37*, 249–258.
Tasdemir, C., Tasdemir, M. A., Lydon, F. D., & Barr, B. I. G. (1996). Effects of silica fume and aggregate size on the brittleness of concrete. *Cement and Concrete Research 26*(1), 63–68.

Tokyay, M., & Ozdemir, M. (1997). Specimen shape and size effect on the compressive strength of higher strength concrete. *Cement and Concrete Research*, *27*, 1281–1289.

Vu, X. H., Daudeville, L., & Malecot, Y. (2011). Effect of coarse aggregate size and cement paste volume on concrete behaviour under high triaxial compression loading. *Construction and Building Materials*, *25*, 3941–3949.

Walker, S., & Bloem, D. L. (1961). *Effect of aggregate size on properties of concrete*. ACI.

Wolinski, S., Hordijk, D. A., Reinhardt, H. W., & Cornelissent, H. A. W. (1987). Influence of aggregate size on fracture mechanics parameters of concrete. *International Journal of Cement Composites*, *9*(2), 95–103.

Wu, Z., Wong, H. S., & Buenfeld, N. R. (2015). Influence of drying-induced microcracking and related size effect on mass transport properties of concrete. *Cement and Concrete Research*, *65*, 35–48.

XP P 18-463. (2011). *Concrete - Testing gas permeability on hardened concrete*. French Standards, AFNOR.

Yazici, S., & Sezer, G. I. (2007). The effect of cylindrical specimen size on the compressive strength of concrete. *Building and Environment*, *42*, 2417–2420.